⌘ *Author's Choice*

Proteomics Characterization of Extracellular Space Components in the Human Aorta*[S]

Athanasios Didangelos‡, Xiaoke Yin‡, Kaushik Mandal§, Mark Baumert¶, Marjan Jahangiri‖, and Manuel Mayr‡**

The vascular extracellular matrix (ECM) is essential for the structural integrity of the vessel wall and also serves as a substrate for the binding and retention of secreted products of vascular cells as well as molecules coming from the circulation. Although proteomics has been previously applied to vascular tissues, few studies have specifically targeted the vascular ECM and its associated proteins. Thus, its detailed composition remains to be characterized. In this study, we describe a methodology for the extraction of extracellular proteins from human aortas and their identification by proteomics. The approach is based on (*a*) effective decellularization to enrich for scarce extracellular proteins, (*b*) successful solubilization and deglycosylation of ECM proteins, and (*c*) relative estimation of protein abundance using spectral counting. Our three-step extraction approach resulted in the identification of 103 extracellular proteins of which one-third have never been reported in the proteomics literature of vascular tissues. In particular, three glycoproteins (podocan, sclerostin, and agrin) were identified for the first time in human aortas at the protein level. We also identified extracellular adipocyte enhancer-binding protein 1, the cartilage glycoprotein asporin, and a previously hypothetical protein, retinal pigment epithelium (RPE) spondin. Moreover, our methodology allowed us to screen for proteolysis in the aortic samples based on the identification of proteolytic enzymes and their corresponding degradation products. For instance, we were able to detect matrix metalloproteinase-9 by mass spectrometry and relate its presence to degradation of fibronectin in a clinical specimen. We expect this proteomics methodology to further our understanding of the composition of the vascular extracellular environment, shed light on ECM remodeling and degradation, and provide insights into important pathological processes, such as plaque rupture, aneurysm formation, and restenosis. ***Molecular & Cellular Proteomics 9: 2048–2062, 2010.***

Vascular cells, in particular vascular smooth muscle cells, produce and maintain a complex meshwork of ECM.[1] The ECM is not only the scaffold for the anchorage and mobility of residing cells but also absorbs and transduces the shear and strain forces of the blood flow. It is primarily composed of elastin, collagen, proteoglycans, and glycoproteins. The elastin fibers and type I and III fibrillar collagens form a rigid network of highly cross-linked interstitial matrix. They offer elasticity (elastin) and tensile strength (collagens). Proteoglycans, because of their negative charge, attract water and confer resistance to compression. Finally, glycoproteins participate in matrix organization and are essential for cell attachment.

The vascular ECM also serves as a substrate for the binding and retention of secreted, soluble proteins of vascular cells as well as molecules coming from the circulation, including lipoproteins, growth factors, cytokines, proteases, and protease inhibitors. These components are invariably associated with ECM proteins, especially proteoglycans. Together they comprise the vascular extracellular environment and are pivotal for disease processes, such as atherosclerosis and aneurysm formation (1).

Although proteomics has been previously applied to vascular tissues, only one study has specifically targeted the extracellular vascular environment (2). This study was focused on the isolation of intimal proteoglycans from human carotid arteries. Moreover, most proteomics studies use whole tissue lysates, which are rich in cellular proteins that inevitably mask the identification of the less abundant proteins of the vascular extracellular environment (3–5). Thus, the composition of the vascular ECM and its associated proteins remains poorly defined. In the present study, we used morphologically normal human aortic samples to develop a method for the extraction of proteins present in the extracellular environment, including ECM proteins and proteins attached to the ECM. We had three specific aims: first, to reduce the contamination with cellular proteins, thereby increasing the chance of identifying scarce extracellular proteins; second, to efficiently solubilize and deglycosylate ECM proteins to improve their analysis by

From the ‡King's British Heart Foundation Centre, King's College, London SE5 9NU, United Kingdom, §Department of Cardiac Surgery, The Johns Hopkins University School of Medicine, Baltimore, Maryland 21205, ¶Advion BioSciences, Harlow CM20 2NQ United Kingdom, ‖Department of Cardiac Surgery, St. George's Healthcare National Health Service Trust, London SW17 0QT, United Kingdom

Received June 10, 2010

⌘ *Author's Choice*—Final version full access.

Published, MCP Papers in Press, June 15, 2010, DOI 10.1074/mcp.M110.001693

[1] The abbreviations used are: ECM, extracellular matrix; MMP, matrix metalloproteinase; GAG, glycosaminoglycan; Bis-Tris, 2-[bis(2-hydroxyethyl)amino]-2-(hydroxymethyl)propane-1,3-diol; ANOVA, analysis of variance; AEBP1, adipocyte enhancer-binding protein 1; RPE, retinal pigment epithelium; LTQ, linear trap quadrupole.

liquid chromatography tandem mass spectrometry (LC-MS/MS); and third, to interface the nanoflow LC system to a recently developed injection device, which splits the flow from the analytical column, to allow the reanalysis of the same sample during a single LC-MS/MS run (RePlay, Advion).

Our methodology provides a detailed overview of the aortic ECM and its associated proteins, many reported for the first time in proteomics analysis of the vasculature. Most importantly, this method could be adapted for use with other tissues to further our understanding of the composition of extracellular environment and ECM turnover under various disease conditions.

EXPERIMENTAL PROCEDURES

Tissue Processing, Decellularization, and Extraction of Extracellular Space Proteins—The data presented were derived from three human aortic samples. The samples were obtained upon aortotomy performed during routine aortic valve replacement. They were collected from positions of the ascending aorta that were free of macroscopically evident vascular pathology, including atherosclerosis or aneurysm formation. The tissue was immediately snap frozen and subsequently kept in liquid nitrogen for later use. A fourth sample was also obtained upon aortotomy and processed as described below, but the proteomics analysis revealed proteolysis of ECM proteins. Therefore, we used it to examine the potential of our methodology to study proteolytic activity in the tissue. All procedures were approved by our local Regional Ethics Committee Board. Informed consent was obtained from all patients recruited into the study.

Before extraction, the tissue pieces were partially thawed and weighed. Approximately 150 mg of tissue per aortic sample were immediately placed in ice-cold phosphate-buffered saline to remove plasma contaminants. Commercially available protease and phosphatase inhibitor mixtures (Sigma-Aldrich) were included according to the manufacturer's instructions to inhibit broad range proteinase activity, and 25 mM EDTA was included to ensure inhibition of metalloproteinases. While the tissue samples were immersed in the cold saline mixture, they were quickly diced with a scalpel into 8–10 smaller pieces. This would enhance (*a*) the initial removal of plasma contaminants and (*b*) the effective extraction of extracellular proteins, which is described below. The saline mixture was changed five times (~30 ml total per sample).

Then, the diced samples were incubated with 0.5 M NaCl, 10 mM Tris, pH 7.5 supplemented with proteinase/phosphatase inhibitor mixtures (Sigma-Aldrich) and 25 mM EDTA. The volume of the buffer was adjusted to 10:1 of the tissue weight (*i.e.* 100 mg in 1 ml), and the samples were mildly vortexed for 4 h at room temperature. The NaCl extracts were then desalted with centrifugation using desalting columns (Zeba Spin, Pierce). Following desalting, the extracts were mixed with 100% acetone (5:1 volume ratio) at −20 °C for 16 h. Proteins were precipitated with centrifugation (16,000 × *g* for 45 min), and the pellets were dried and redissolved in deglycosylation buffer (see below).

Subsequently, the aortic samples were incubated with 0.08% SDS (10:1 buffer volume to tissue weight) supplemented with proteinase/phosphatase inhibitor mixtures and 25 mM EDTA. The samples were mildly vortexed for 4 h at room temperature to achieve removal of cellular components. From our experience with tissue extractions, we took particular care to ensure a low vortexing speed to decrease the possibility of mechanical disruption of the ECM. The SDS solution was then removed and stored frozen for later use.

Finally, the samples were incubated in a 4 M guanidine HCl, 50 mM sodium acetate, pH 5.8 buffer (5:1 buffer volume to tissue weight) supplemented with proteinase/phosphatase inhibitor mixtures and 25 mM EDTA. Adjusting the pH to 5.8 is important; more than 30 years ago it was shown that at this pH guanidine is more effective in solubilizing vascular proteoglycans, whereas higher pH is required for the solubilization of the proteoglycans from other ECM-rich tissues, such as cartilage (6). The samples were then incubated for 48 h at room temperature and vortexed vigorously to enhance mechanical disruption of the ECM components. Subsequently, the guanidine extracts were mixed with 100% ethanol (5:1 volume ratio) at −20 °C for 16 h to ensure removal of guanidine (the presence of guanidine would hinder further biochemical processing). Proteins were precipitated with centrifugation (16,000 × *g* for 45 min), and the pellets were washed with 90% ethanol, dried, and redissolved in deglycosylation buffer (see below).

Deglycosylation (removal of glycosaminoglycan side chains) of the different extracts was achieved in a 150 mM NaCl, 50 mM sodium acetate, pH 6.8 buffer supplemented with proteinase/phosphatase inhibitors and 10 mM EDTA for 16 h at 37 °C. The deglycosylation enzymes (0.05 unit) used were chondroitinase ABC from *Proteus vulgaris* (It catalyzes the removal of polysaccharides containing 1→4-β-D-hexosaminyl and 1→3-β-D-glucuronosyl or 1→3-α-L-iduronosyl linkages to disaccharides containing 4-deoxy-β-D-gluc-4-enuronosyl groups. It acts on chondroitin 4-sulfate, chondroitin 6-sulfate, and dermatan sulfate glycosaminoglycan side chains.), keratanase from *Bacteroides fragilis* (cleaves internal 1→4-β-galactose linkages in unbranched, repeating poly-*N*-acetyl-lactosamine and keratan sulfate), and heparitinase II from *Flavobacterium heparinum* (cleaves heparan sulfate), all purchased from Sigma-Aldrich. Following deglycosylation, the solutions were clarified again with centrifugation (16,000 × *g* for 10 min) to ensure that the samples were free of turbidity, and protein concentration was estimated by UV absorbance at 280 nm using extinction coefficient of 1.1 of 0.1% mg/ml solution calculated on the basis of the frequency of tyrosine and tryptophan, which are the main UV light-absorbing amino acids at 280 nm in mammalian proteins (7).

One-dimensional Electrophoresis—The NaCl, guanidine, and SDS extracts were denatured and reduced in sample buffer containing 100 mM Tris, pH 6.8, 40% glycerol, 0.2% SDS, 2% β-mercaptoethanol, and 0.02% bromphenol blue and boiled at 96 °C for 10 min. 35 μg of protein per sample were loaded and separated on Bis-Tris discontinuous 4–12% polyacrylamide gradient gels (NuPAGE, Invitrogen). Prestained protein standards were run alongside the samples to allow molecular mass estimation of proteins (All Blue, Precision Plus, Bio-Rad).

Nanoflow LC-MS/MS for NaCl and Guanidine Extracts—After electrophoresis, gels were stained using the PlusOne Silver staining kit (GE Healthcare). Silver staining was used for band excision to avoid cross-contamination with fainter gel bands. (Coomassie staining will predominantly stain the abundant proteins; hence, fainter gel bands could be missed.). The gel bands were excised in identical parallel positions across lanes, and no "empty" gel pieces were left behind. Subsequently, all gel bands were subjected to in-gel digestion with trypsin using an Investigator ProGest (Genomic Solutions) robotic digestion system. Tryptic peptides from the NaCl and guanidine extracts were separated on a nanoflow LC system (Dionex UltiMate 3000) and eluted with a 40-min gradient (10–25% B in 35 min, 25–40% B in 5 min, 90% B in 10 min, and 2% B in 30min where A is 2% ACN, 0.1% formic acid in HPLC H_2O and B is 90% ACN, 0.1% formic acid in HPLC H_2O). The column (Dionex PepMap C_{18}, 25-cm length, 75-μm internal diameter, 3-μm particle size) was coupled to a nanospray source (Picoview) using RePlay (Advion). After the direct LC-MS run, the flow was switched, and the portion stored in the capillary of the RePlay device was reanalyzed ("replay run") (8). Spectra were collected from an ion trap mass analyzer (LTQ-Orbitrap XL, Thermo Fisher Scientific) using full ion scan mode over the mass-to-

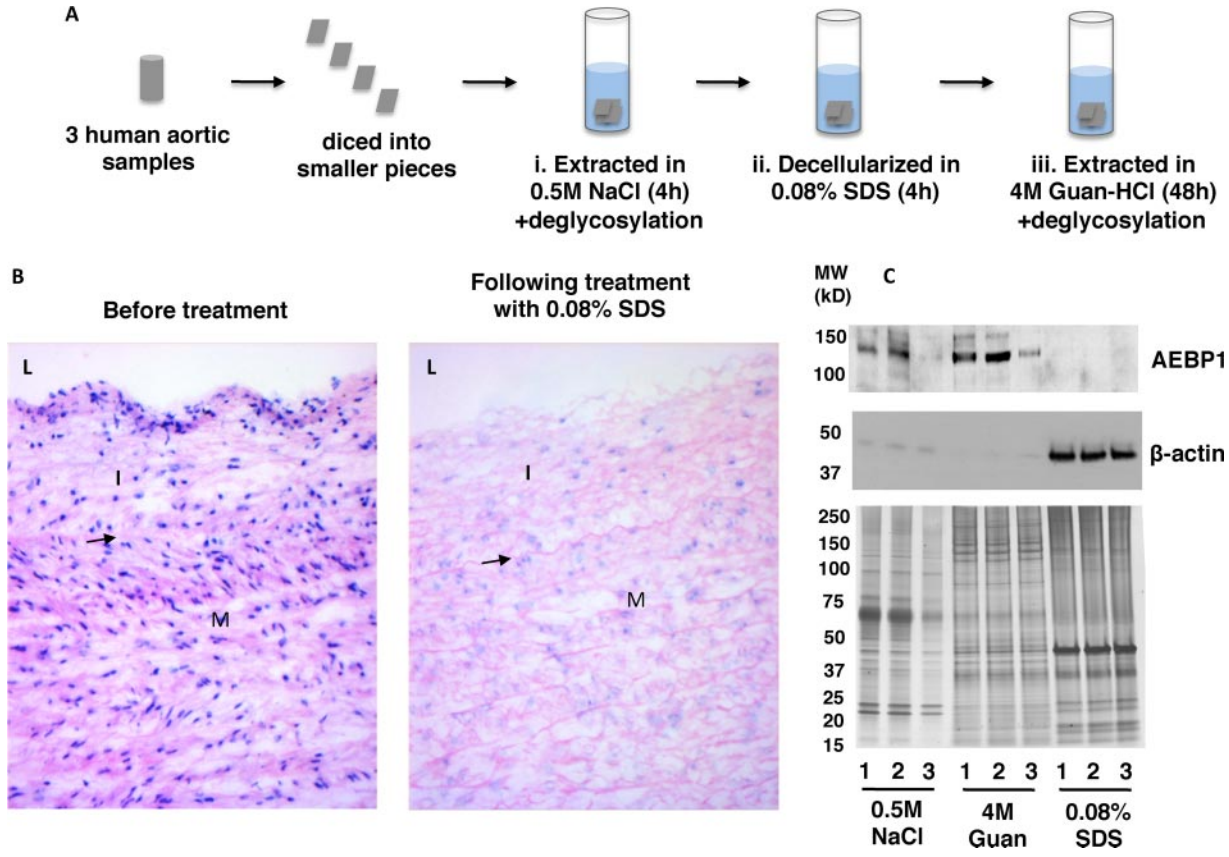

FIG. 1. **Identification of extracellular proteins in human aortas.** *A*, schematic summary. Biochemical subfractionation was used for the enrichment of extracellular space proteins before proteomic analysis. *B*, validation of decellularization by hematoxylin/eosin staining. Representative images of a hematoxylin/eosin-stained human aorta before (*left panel*) and after decellularization with 0.08% SDS (*right panel*) are shown. *L*, lumen; *I*, intima; *M*, media. *Arrows* depict the intima/media border. Note the loss of nuclear (*blue*; hematoxylin) and cytoplasmic contents (*pink*; eosin), whereas other eosinophilic structures, such as collagen fibers, are preserved. *C*, immunoblotting and silver staining. The ECM glycoprotein AEBP1 is found in the NaCl and guanidine (*Guan*) extracts, which are enriched in proteins of the extracellular space (*upper panel*). Cytoplasmic β-actin is predominantly found in the SDS extracts (*middle panel*), demonstrating successful depletion of cellular contents. Silver staining of proteins from all extracts separated by one-dimensional SDS-PAGE shows the pattern of proteins extracted in the three different extraction steps (*bottom panel*).

charge (*m/z*) range 450–1600. MS/MS was performed on the top six ions in each MS scan using the data-dependent acquisition mode with dynamic exclusion enabled. MS/MS peak lists were generated by extract_msn.exe and matched to a human database (UniProtKB/Swiss-Prot Release 14.6, 20,333 protein entries) using SEQUEST version 28 (revision 13) (Bioworks Browser 3.3.1 SP1, Thermo Fisher Scientific) and X! Tandem (version 2007.01.01.2). Carboxyamidomethylation of cysteine was chosen as a fixed modification, and oxidation of methionine was chosen as a variable modification. The mass tolerance was set at 1.5 amu for the precursor ions and at 1.0 amu for fragment ions. Two missed cleavages were allowed. Scaffold (version 2.0.5, Proteome Software Inc., Portland, OR) was used to calculate the spectral counts and to validate MS/MS-based peptide and protein identifications (9, 10). According to the default values in the Scaffold software, the following peptide thresholds were applied: X! Tandem: $-\log(\text{Expect scores}) > 2.0$; SEQUEST: $\Delta Cn > 0.10$ and $XCorr > 2.5$ (2+), 3.5 (3+), and 3.5 (4+). Peptide identifications were accepted if they could be established at greater than 95.0% probability as specified by the Peptide Prophet algorithm (9). Protein identifications were accepted if they could be established at greater than 99.0% probability (10) with at least two independent peptides and a precursor ion mass accuracy ≤10 ppm.

Nanoflow LC-MS/MS for SDS Extracts—The protein concentration in the SDS extracts was estimated using the Groves equation, $(A_{280} \times 1.55) - (A_{260} \times 0.76)$ (11), which takes into account nucleic acid interference. 35 μg of protein per sample were loaded and separated on Bis-Tris discontinuous 4–12% polyacrylamide gradient gels as above. The gel was silver-stained, and protein bands were digested by trypsin as described above. Tryptic peptides were separated on a split-free, nanoflow LC system (EASY-nLC, Proxeon) on a C_{18} column (Easy-nLC C_{18}, Proxeon, 10-cm length, 75-μm internal diameter, 3-μm particle size) and eluted with an 80-min gradient (10–25% B in 35 min, 25–40% B in 5 min, 90% B in 10 min, and 2% B in 30min where A is 2% ACN, 0.1% formic acid in HPLC H_2O and B is 90% ACN, 0.1% formic acid in HPLC H_2O). The nanoflow LC system was not coupled to a RePlay device. Spectra were collected from a dual pressure, linear ion trap (LTQ Velos, Thermo Fisher Scientific) using full ion scan mode over the *m/z* range 300–1800. MS/MS was performed on the top 20 ions in each MS scan using the data-dependent acquisition mode with dynamic exclusion enabled. MS/MS peak lists were generated by extract_msn.exe and matched to a human database (UniProtKB/Swiss-Prot Release 15.13, 20,276 protein entries) using SEQUEST version 28 (revision 13) (Proteome Discoverer 1.2 beta, Thermo Fisher Scientific). Carboxyamidomethylation of cysteine

TABLE I

Extracellular space proteins identified by proteomics in three NaCl extracts

COMP, cartilage oligomeric matrix protein; IGF, insulin-like growth factor.

Protein name	Swiss-Prot accession name	Molecular mass	Unique peptides, *n*	Unique spectra, *n*	Coverage	Total spectra,[a] *n*
		kDa			%	
Proteoglycans and glycoproteins						
Lumican	LUM_HUMAN	38	40	40	20.0	249
Tenascin-X	TENX_HUMAN	464	66	66	8.1	156
Fibulin-3	FBLN3_HUMAN	55	38	38	22.0	155
Adipocyte enhancer-binding protein 1[b]	AEBP1_HUMAN	131	37	39	11.0	153
Fibronectin	FINC_HUMAN	263	34	34	7.3	111
Perlecan	PGBM_HUMAN	469	16	16	2.5	50
Mimecan	MIME_HUMAN	34	13	13	12.0	49
Versican	CSPG2_HUMAN	373	16	16	3.7	46
Tetranectin	TETN_HUMAN	23	20	20	29.0	39
Fibromodulin	FMOD_HUMAN	43	6	6	7.4	26
Fibulin-1	FBLN1_HUMAN	77	14	14	9.1	25
Latent TGFβ-binding protein 2[b]	LTBP2_HUMAN	195	15	15	5.2	23
Thrombospondin-1	TSP1_HUMAN	129	11	11	5.1	18
Podocan[b]	PODN_HUMAN	69	10	10	6.9	17
Fibrillin-1	FBN1_HUMAN	312	10	10	2.1	16
Fibulin-5	FBLN5_HUMAN	50	6	6	7.8	12
Galectin-1	LEG1_HUMAN	15	7	7	26.0	9
Decorin	PGS2_HUMAN	40	3	3	10.0	8
Latent TGFβ-binding protein 4[b]	LTBP4_HUMAN	173	3	3	1.6	7
Clusterin	CLUS_HUMAN	52	3	3	3.6	5
COMP	COMP_HUMAN	83	2	2	6.3	3
Tenascin	TENA_HUMAN	241	2	2	0.95	2
Dermatopontin	DERM_HUMAN	24	2	2	9.5	2
Other ECM-associated proteins						
Extracellular superoxide dismutase	SODE_HUMAN	26	22	27	46.0	209
Pigment epithelium-derived factor	PEDF_HUMAN	46	32	32	16.0	82
Serum amyloid P-component	SAMP_HUMAN	25	31	31	26.0	62
IGF-binding protein 7[b]	IBP7_HUMAN	29	15	15	21.0	47
Apolipoprotein A-I	APOA1_HUMAN	31	6	6	25.0	19
Apolipoprotein A-IV	APOA4_HUMAN	45	7	7	17.0	12
Apolipoprotein H[b]	APOH_HUMAN	38	8	8	14.0	11
Hepatoma-derived growth factor[b]	HDGF_HUMAN	27	6	6	7.9	11
Secreted frizzled-related protein 1[b]	SFRP1_HUMAN	35	5	5	9.2	9
Ceruloplasmin	CERU_HUMAN	122	4	4	2.3	9
Secreted frizzled-related protein 3[b]	SFRP3_HUMAN	36	4	4	9.2	8
Apolipoprotein D	APOD_HUMAN	21	6	6	20.0	8
Apolipoprotein E	APOE_HUMAN	36	5	5	7.6	7
LIM and cysteine-rich domains protein 1[b]	LMCD1_HUMAN	41	6	6	7.7	7
Spondin-1[b]	SPON1_HUMAN	91	3	3	2.7	6
Target of Nesh-SH3[b]	TARSH_HUMAN	119	2	2	2.6	6
Proteases and protease inhibitors						
Tryptase β-1[b]	TRYB1_HUMAN	31	9	9	22.0	22
Procollagen C-endopeptidase enhancer 1	PCOC1_HUMAN	48	8	8	7.8	18
Cathepsin G[b]	CATG_HUMAN	29	7	7	6.7	16
Calreticulin	CALR_HUMAN	48	9	9	11.0	13
Cathepsin Z[b]	CATZ_HUMAN	34	6	6	7.3	10
Plasma glutamate carboxypeptidase[b]	PGCP_HUMAN	52	5	5	4.2	8
Cathepsin D	CATD_HUMAN	45	5	5	7.0	7
Leukocyte elastase inhibitor	ILEU_HUMAN	43	5	5	9.0	7
Proactivator polypeptide[b]	SAP_HUMAN	58	5	5	5.3	7
MMP-2[b]	MMP2_HUMAN	74	2	2	3.3	4
Kallistatin[b]	KAIN_HUMAN	49	2	2	4.7	3
Carboxypeptidase-like protein X2[b]	CPXM2_HUMAN	86	2	2	4.6	2

TABLE I—*continued*

Protein name	Swiss-Prot accession name	Molecular mass	Unique peptides, *n*	Unique spectra, *n*	Coverage	Total spectra,[a] *n*
		kDa			%	
Collagens						
Collagen α-1(XIV)[b]	COEA1_HUMAN	194	73	73	14.0	233
Collagen α-1(XII)	COCA1_HUMAN	333	20	20	2.8	41
Collagen α-3(VI)	CO6A3_HUMAN	344	16	16	3.7	29
Collagen α-1(XVIII)	COIA1_HUMAN	178	11	11	3.7	22
Collagen α-2(VI)	CO6A2_HUMAN	109	4	4	3.0	6
Collagen α-1(XV)	COFA1_HUMAN	142	3	3	2.0	4
Collagen α-1(I)	CO1A1_HUMAN	129	3	3	1.5	4

[a] Sum of all spectra identified for each protein in the three biological samples, performed with two technical replicates each.
[b] Proteins found for the first time by proteomics in the vasculature.

was chosen as a fixed modification, and oxidation of methionine was chosen as a variable modification. The mass tolerance was set at 0.5 amu for the precursor ions and at 0.5 amu for fragment ions. Two missed cleavages were allowed. Scaffold (version 3, Proteome Software Inc.) was used to calculate the spectral counts and to validate MS/MS-based peptide and protein identifications as before. According to the default values in the Scaffold software, the following peptide thresholds were applied: SEQUEST: $\Delta Cn > 0.10$ and $XCorr > 2.5$ (2+), 3.5 (3+), and 3.5 (4+). Peptide identifications were accepted if they could be established at greater than 95.0% probability as specified by the Peptide Prophet algorithm (9). Protein identifications were accepted if they could be established at greater than 99.0% probability (10) with at least two independent peptides.

Western Blotting—Aliquots of the NaCl, guanidine, and SDS extracts were mixed with denaturing sample buffer and boiled. 20 μg of protein per sample were loaded and separated on 4–12% gradient gels as above. Proteins were then transferred on nitrocellulose membranes. Membranes were blocked in 5% fat-free milk powder in PBS and then probed for 16 h at 4 °C with primary antibodies to β-actin (sc-130656), periostin (sc-67233), and fibronectin (sc-56391). The antibodies were purchased from Santa Cruz Biotechnology and were used at a 1:500 dilution in 5% BSA. The membranes were then treated with the appropriate secondary, peroxidase-conjugated antibodies (Dako) at a 1:2000 dilution. Finally, the blots were imaged using enhanced chemiluminescence (ECL; GE Healthcare), and films were developed on a Xograph processor. The densitometry for the lanes from developed blots for periostin and asporin was performed using ImageJ software.

Gelatinolytic Zymography—Gelatinolytic zymograms were used to detect the presence of MMP-2 and -9 in the 0.5 M NaCl extracts. Extract aliquots (20 μg of protein) were mixed with non-reducing sample buffer containing 100 mM Tris, pH 6.8, 40% glycerol, 0.2% SDS, and 0.02% bromphenol blue and separated by 10% SDS-PAGE in gels containing 0.5 mg/ml gelatin (Sigma-Aldrich). Prestained protein standards were run alongside the samples as before. To allow in-gel MMP activity, SDS was removed from the gels with three washes in a buffer containing 2% Triton X-100, 50 mM Tris, pH 7.4, and 200 mM NaCl for 45 min. Gels were then incubated for 16 h to detect MMP-9 or 36 h to detect MMP-2 at 37 °C in a buffer containing 50 mM Tris, pH 7.4, 200 mM NaCl, and 10 mM $CaCl_2$. Finally, gels were stained for 60 min with Coomassie Brilliant Blue (Sigma-Aldrich) and destained for 2 h to visualize the MMPs.

Histochemistry—Small representative pieces from each aortic sample were placed in optimal cutting temperature (OCT) compound (BDH), which was subsequently frozen. The frozen tissue blocks were used to generate consecutive 7-μm-thick cross-sections. The sections were air-dried (30 min) and fixed in 100% acetone for 20 min. Subsequently, sections were used either to generate hematoxylin- and eosin-stained histological slides or for immunohistochemical analysis using antibodies to podocan used at 2 μg/ml (MAB4220) (R&D Systems), sclerostin (sc-130258) used at 1 μg/ml, and agrin (sc-25528) used at used at 2 μg/ml (Santa Cruz Biotechnology). Negative controls were generated with either mouse (podocan) or rabbit (sclerostin and agrin) isotype IgG antibodies (Sigma-Aldrich) used at 2 μg/ml. The immunostaining was generated using the DAB+ (diaminobenzidine) peroxidase-based chromogen system (Dako) according to the manufacturer's instructions. Images were taken by a Zeiss Axioplan 2ie microscope interfaced to AxioVision software (version 3.0.6).

Statistical Analysis of NaCl and Guanidine Extracts—For each clinical sample ($n = 4$) and biochemical fraction ($n = 2$) analyzed, we obtained a technical replicate by using the RePlay device. The reproducibility of the RePlay analysis was assessed by calculating the Pearson correlation coefficient for the spectral counts. All spectra from proteins identified with at least two unique peptides were included in the analysis, and no outliers were removed. The *p* value for the linear dependence between the RePlay runs was obtained using the Fisher transformation. To assess biological variability among the four clinical specimens, we computed the coefficient of variation for all identified proteins using Scaffold software (version 2.0.5, Proteome Software Inc.). A coefficient of variation exceeding 100% was applied as a cutoff. Statistical significance was determined by using analysis of variance (ANOVA). A p value <0.05 was considered significant.

RESULTS

Biochemical Extraction of Proteins in Extracellular Environment—Our extraction methodology was developed on human aortic samples obtained during cardiac surgery for aortic valve replacement of degenerative aortic valve stenosis. Fig. 1*A* is a schematic summary of the methodology used in this study. The samples ($n = 3$) were macroscopically classified as normal during surgery, and upon histological examination, they showed no pathological signs. Extraction of the proteins of the vascular extracellular environment and reduction of the contamination with cellular proteins were achieved by a three-step extraction procedure. First, the tissue samples were treated with 0.5 M NaCl. The salt ions induce displacement of polyionic interactions between proteins, thus enabling the extraction of loosely bound extracellular proteins, including newly synthesized ECM proteins and degradation products

TABLE II

Extracellular space proteins identified by proteomics in three guanidine extracts

IGF, insulin-like growth factor.

Protein name	Swiss-Prot accession name	Molecular mass	Unique peptides, *n*	Unique spectra, *n*	Coverage	Total spectra,[a] *n*
		kDa			%	
Proteoglycans and glycoproteins						
Perlecan	PGBM_HUMAN	469	367	481	19.0	1596
Fibronectin	FINC_HUMAN	263	182	218	20.0	1028
Versican	CSPG2_HUMAN	373	76	89	4.4	681
Aggrecan	PGCA_HUMAN	250	70	82	6.3	451
Biglycan	PGS1_HUMAN	42	56	62	36.0	352
Lactadherin	MFGM_HUMAN	43	64	67	48.0	309
Prolargin	PRELP_HUMAN	44	55	78	37.0	283
Periostin	POSTN_HUMAN	93	100	117	29.0	257
Lumican	LUM_HUMAN	38	53	58	30.0	204
Decorin	PGS2_HUMAN	40	43	51	29.0	173
Clusterin	CLUS_HUMAN	52	44	48	23.0	173
Tenascin-X	TENX_HUMAN	464	79	79	4.5	140
Laminin subunit γ-1	LAMC1_HUMAN	178	40	44	18.0	129
Link protein 1	HPLN1_HUMAN	40	26	29	33.0	117
Laminin subunit β-2	LAMB2_HUMAN	196	34	34	14.0	104
Vitronectin	VTNC_HUMAN	54	25	27	14.0	102
Nidogen-1	NID1_HUMAN	136	56	64	15.0	101
Adipocyte enhancer-binding protein 1[b]	AEBP1_HUMAN	131	34	40	7.6	94
Laminin subunit α-5	LAMA5_HUMAN	400	39	39	4.6	91
Tenascin	TENA_HUMAN	241	25	25	5.6	52
Mimecan	MIME_HUMAN	34	21	21	15.0	48
EGF-containing fibulin-like ECM protein 1	FBLN3_HUMAN	55	22	24	15.0	48
Fibulin-5	FBLN5_HUMAN	50	17	17	14.0	40
Galectin-1	LEG1_HUMAN	15	17	20	53.0	40
TGFβ-induced protein ig-h3	BGH3_HUMAN	75	23	23	12.0	35
EMILIN-1	EMIL1_HUMAN	107	8	8	3.0	30
Fibulin-1	FBLN1_HUMAN	77	17	17	12.0	29
Latent TGFβ-binding protein 2[b]	LTBP2_HUMAN	195	13	13	2.7	22
Fibromodulin	FMOD_HUMAN	43	8	11	8.2	22
Microfibril-associated glycoprotein 4	MFAP4_HUMAN	29	8	8	12.0	21
Dermatopontin	DERM_HUMAN	24	8	9	12.0	21
Fibrillin-1	FBN1_HUMAN	312	15	15	2.4	21
Latent TGFβ-binding protein 4[b]	LTBP4_HUMAN	173	12	12	4.2	15
Nidogen-2	NID2_HUMAN	151	8	8	3.5	11
Agrin[b]	AGRIN_HUMAN	215	7	7	2.3	11
Asporin	ASPN_HUMAN	43	8	8	11.0	11
Cartilage oligomeric matrix protein	COMP_HUMAN	83	4	4	3.6	7
Thrombospondin-1	TSP1_HUMAN	129	3	3	1.8	7
Matrix Gla protein	MGP_HUMAN	12	4	4	13.0	6
Galectin-3	LEG3_HUMAN	26	2	2	6.0	4
Sclerostin[b]	SOST_HUMAN	24	2	2	5.6	3
Matrilin-2[b]	MATN2_HUMAN	107	2	2	2.3	3
Other ECM-associated proteins						
Serum amyloid P-component	SAMP_HUMAN	25	32	33	33.0	169
Tubulointerstitial nephritis antigen-like[b]	TINAL_HUMAN	52	46	55	21.0	131
Extracellular superoxide dismutase	SODE_HUMAN	26	28	35	25.0	102
Target of Nesh-SH3[b]	TARSH_HUMAN	119	30	33	8.6	89
IGF-binding protein 7[b]	IBP7_HUMAN	29	30	31	28.0	59
Cysteine-rich protein 2	CRIP2_HUMAN	22	20	21	25.0	57
TGFβ-1-induced transcript 1 protein[b]	TGFI1_HUMAN	50	27	27		45
LIM and cysteine-rich domains protein 1[b]	LMCD1_HUMAN	41	25	25	34.0	39
Apolipoprotein H[b]	APOH_HUMAN	38	10	12	9.0	32
Galectin-3-binding protein	LG3BP_HUMAN	65	12	12	12.0	23
RPE-spondin[b]	RPESP_HUMAN	30	12	12	22.0	19

TABLE II—*continued*

Protein name	Swiss-Prot accession name	Molecular mass	Unique peptides, *n*	Unique spectra, *n*	Coverage	Total spectra,[a] *n*
		kDa			%	
Carboxypeptidase-like protein X2[b]	CPXM2_HUMAN	86	9	11	7.3	16
Latent TGFβ-binding protein, isoform 1S[b]	LTB1S_HUMAN	153	8	9	2.7	13
Pigment epithelium derived factor	PEDF_HUMAN	46	5	5	8.6	8
Secreted frizzled-related protein 1[b]	SFRP1_HUMAN	35	3	3	8.9	6
Properdin[b]	PROP_HUMAN	51	3	4	5.1	5
Spondin-1[b]	SPON1_HUMAN	91	3	3	3.0	4
Neutrophil defensin 1[b]	DEF1_HUMAN	10	2	2	9.6	4
Proteases and protease inhibitors						
Serine protease HTRA1	HTRA1_HUMAN	51	22	22	13.0	68
Chymase[b]	CMA1_HUMAN	27	12	15	11.0	23
Lysyl oxidase homolog 1[b]	LOXL1_HUMAN	63	12	12	7.3	23
Metalloproteinase inhibitor 3	TIMP3_HUMAN	24	9	9	17.0	12
Tryptase β-1[b]	TRYB1_HUMAN	31	6	7	9.8	11
Procollagen C-endopeptidase enhancer 1	PCOC1_HUMAN	48	7	7	6.7	10
Cathepsin G[b]	CATG_HUMAN	29	7	7	15.0	8
Cathepsin D	CATD_HUMAN	45	4	4	2.7	7
Antileukoproteinase[b]	SLPI_HUMAN	14	3	3	9.1	6
Myeloblastin[b]	PRTN3_HUMAN	28	2	2	4.7	4
Collagens						
Collagen α-3(VI)	CO6A3_HUMAN	344	164	186	20.0	898
Collagen α-1(XIV)[b]	COEA1_HUMAN	194	136	150	20.0	529
Collagen α-1(XVIII)	COIA1_HUMAN	178	45	48	5.9	374
Collagen α-1(VI)	CO6A1_HUMAN	109	50	71	16.0	282
Collagen α-2(VI)	CO6A2_HUMAN	109	31	31	19.0	155
Collagen α-2(IV)	CO4A2_HUMAN	168	26	31	3.9	139
Collagen α-1(XV)	COFA1_HUMAN	142	32	34	7.5	100
Collagen α-1(XII)	COCA1_HUMAN	333	42	42	4.0	90
Collagen α-2(I)	CO1A2_HUMAN	129	12	15	3.5	70
Collagen α-1(I)	CO1A1_HUMAN	139	14	15	5.9	51
Collagen α-1(VIII)	CO8A1_HUMAN	73	5	5	1.3	33
Collagen α-1(V)	CO5A1_HUMAN	184	6	6	0.6	23
Collagen α-2(VIII)	CO8A2_HUMAN	67	4	4	3.3	9
Collagen α-1(IV)	CO4A1_HUMAN	161	5	5	1.8	8

[a] Sum of all spectra identified for each protein in the three biological samples, performed with two technical replicates each.
[b] Proteins found for the first time by proteomics in the vasculature.

(12), providing an overview of tissue turnover. The tissue was then decellularized using SDS. In contrast to other decellularization reagents, such as non-ionic detergents (Triton X-100) (13), 0.1% SDS has been previously shown to be very effective in solubilizing cytoplasmic and nuclear membranes, thereby removing cellular components from tissues (14). However, the ionic detergent above its critical micelle concentration can also cause protein denaturation and disrupt native ECM proteins (15).

To substantially remove the cellular material while preserving the ECM and its associated proteins as much as possible, we used 2.8 mM (0.08%) SDS in distilled water. This concentration is well below the critical micelle concentration of SDS in distilled water, which is 8 mM (16). In addition, at this concentration, SDS is effective in solubilizing cell membrane lipid bilayers (17). Treatment with 0.08% SDS was sufficient to remove most cellular components as shown by the marked reduction of nuclear staining (hematoxylin; Fig. 1*B*, *blue*). The cytoplasmic staining (eosin; *pink*) was also reduced, but other eosinophilic structures, such as collagen and elastin, were preserved in the tissue. Finally, the specimens were subjected to denaturing extraction in a 4 M guanidine HCl buffer. Guanidine HCl extractions were developed more than 40 years ago as a very effective way to solubilize most of the strongly bound ECM components, including large aggregating proteoglycans (versican, aggrecan, etc.), small proteoglycans (decorin, biglycan, etc.), cell attachment matrix glycoproteins (such as type VI collagen, fibronectins, and laminins), and basement membrane components (perlecan, type IV collagen, etc.). Guanidine induces disaggregation of ECM components by destabilizing the ionic, disulfide-dependent protein conformations (18). Following dissociative extraction, only the insoluble, heavily cross-linked interstitial matrix, namely type I and III collagens and elastin, remains in the tissue. Western blotting confirmed that β-actin immunoreactivity is predominantly found in the SDS extracts (Fig 1*C*, *middle panel*), which also had the highest protein concentration per milliliter (supplemental Fig. 1). On the other hand, the extracellular

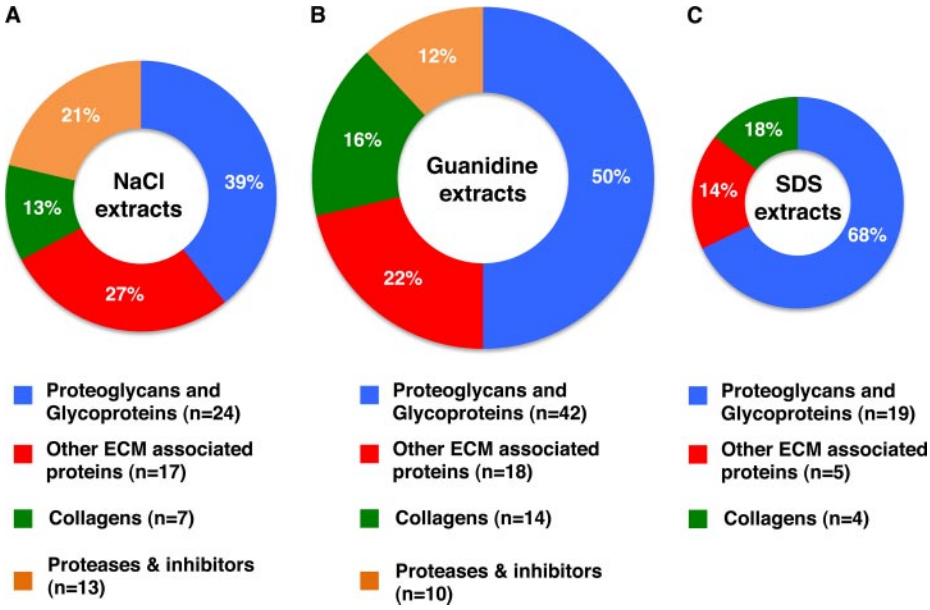

FIG. 2. **Protein categories.** The classification and numerical distribution of the identified extracellular proteins in the NaCl (*A*), guanidine (*B*), and SDS (*C*) extracts are shown. The *size* of the *doughnut charts* is representative of the number of extracellular space proteins identified in the different extracts.

TABLE III
Extracellular space proteins identified by proteomics in three SDS extracts

Protein name	Swiss-Prot accession name	Molecular mass	Unique peptides, *n*	Unique spectra, *n*	Coverage	Total spectra,[a] *n*
		kDa			%	
Proteoglycans and glycoproteins						
Biglycan	PGS1_HUMAN	42	24	28	32.6	141
Decorin	PGS2_HUMAN	40	24	24	33.1	85
Mimecan	MIME_HUMAN	34	21	22	15.0	76
Lumican	LUM_HUMAN	38	17	18	24.6	72
Prolargin	PRELP_HUMAN	44	19	19	22.5	59
Fibronectin	FINC_HUMAN	263	29	29	8.1	38
Versican	CSPG2_HUMAN	373	13	13	2.3	33
Lactadherin	MFGM_HUMAN	43	13	15	21.2	23
Perlecan	PGBM_HUMAN	469	20	20	2.9	22
Clusterin	CLUS_HUMAN	52	7	7	14.2	18
EGF-containing fibulin-like ECM protein 1	FBLN3_HUMAN	55	6	6	10.6	11
Periostin	POSTN_HUMAN	93	7	7	4.8	11
Galectin-1	LEG1_HUMAN	15	5	5	23.0	7
Tenascin	TENA_HUMAN	241	5	5	2.1	6
Vitronectin	VTNC_HUMAN	54	4	4	5.6	5
Link protein 1	HPLN1_HUMAN	40	4	4	13.0	5
Fibulin-1	FBLN1_HUMAN	77	3	3	3.8	3
Laminin subunit α-4	LAMA4_HUMAN	203	3	3	1.9	3
Fibulin-5	FBLN5_HUMAN	50	3	3	6.0	3
Other ECM-associated proteins						
Apolipoprotein E	APOE_HUMAN	36	12	12	17.7	18
Extracellular superoxide dismutase	SODE_HUMAN	26	10	10	24.0	13
Apolipoprotein B	APOD_HUMAN	21	7	7	1.5	10
Apolipoprotein A-I	APOA1_HUMAN	30	5	5	15.0	5
Galectin-3-binding protein	LG3BP_HUMAN	65	3	3	6.7	3
Collagens						
Collagen α-3(VI)	CO6A3_HUMAN	344	57	58	7.4	109
Collagen α-2(VI)	CO6A2_HUMAN	109	11	11	2.4	20
Collagen α-1(XIV)[b]	COEA1_HUMAN	194	7	7	3.6	8
Collagen α-1(XVIII)	COIA1_HUMAN	178	6	6	1.5	7

[a] Sum of all spectra identified for each protein in the three biological samples, performed with two technical replicates each.
[b] Proteins found for the first time by proteomics in the vasculature.

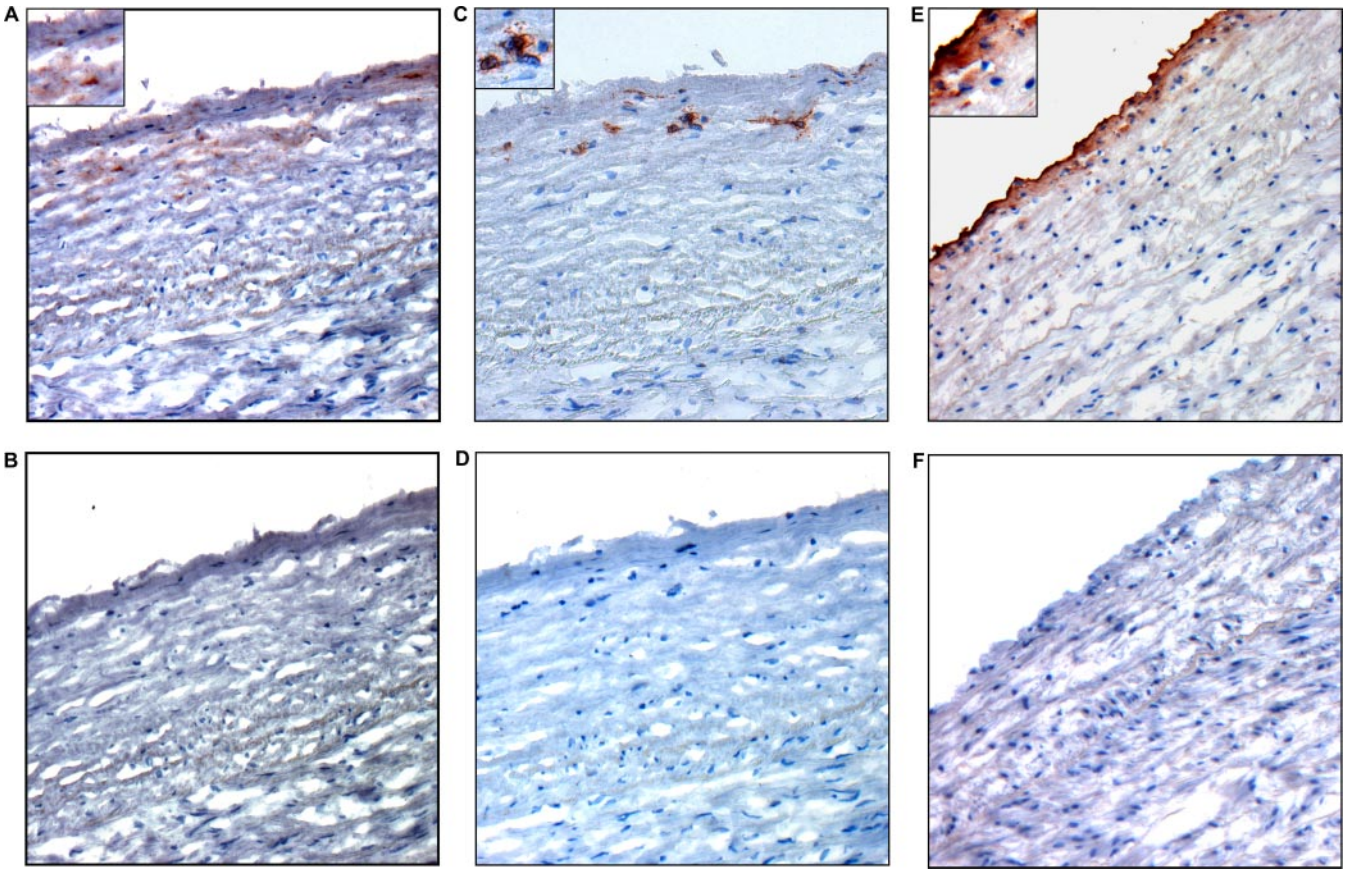

FIG. 3. **Confirmation of podocan, sclerostin, and agrin in aortic ECM.** Immunohistological staining confirmed the presence of podocan in the aortic intima (*A*). Immunoreactivity appears in *brown* (*magnification*, 20×; *inset magnification*, 60×). Nuclei are counterstained with Mayer's hematoxylin (*blue*). Sclerostin (*C*) was localized in the subendothelial layer of the aortic intima. Finally, immunohistochemical staining confirmed the presence of agrin (*E*). Agrin is localized on the aortic endothelium. The respective isotype negative controls are shown in *B*, *D*, and *F*, respectively. The specificity of the sclerostin and agrin antibodies was confirmed by immunoblotting (data not shown). The aortic specimens were from a 44-year old female (*A*, *B*) and a 55-year old male patient (*C–F*).

AEBP1 isoform, an ECM-associated glycoprotein, was detected in the NaCl and guanidine extracts by Western blotting (Fig 1*C*, *upper panel*), indicating that these extracts are enriched in proteins of the extracellular space. Silver staining revealed a distinct but reproducible protein pattern in the three different extraction steps (Fig. 1*C*, *bottom panel*).

The different extracts were subjected to enzymatic deglycosylation to remove chondroitin, keratan, and heparan sulfate glycosaminoglycan (GAG) chains from the matrix glycoproteins. Deglycosylation is a critical step in our methodology. First, GAGs increase the molecular weight of glycoproteins and affect their separation and resolution by one-dimensional electrophoresis. Second, the presence of GAGs greatly reduces the chance for the identification of proteoglycans by mass spectrometry.

Proteomics Analysis of Extracts—After separation by SDS-PAGE, protein bands were excised from silver-stained gels, subjected to in-gel tryptic digestion, and analyzed by LC-MS/MS. The peptides were injected into a high mass accuracy ion trap (LTQ-Orbitrap XL, Thermo Fisher Scientific) using RePlay (Advion). This injection system splits the gradient from the analytical column and allows the reanalysis of the same sample in a single LC-MS/MS run (8). 272 and 321 proteins were identified in the NaCl and guanidine extracts, respectively. All the peptides identified by LC-MS/MS in the NaCl and guanidine extracts are shown in supplemental Tables 1 and 2. According to their gene ontology annotation (European Molecular Biology Laboratory-European Bioinformatics Institute database, www.uniprot.org), a quarter of these proteins were located in the extracellular space: among the 61 extracellular proteins in the NaCl extracts (Table I) and the 84 extracellular proteins in the guanidine extracts (Table II), proteins highlighted with Footnote b were, to the best of our knowledge, identified for the first time in the vasculature by proteomics. Lipoproteins were included (even though they are plasma-derived) because of their intimate relationship with proteoglycans and their relevance in cardiovascular pathology. The classification of the identified extracellular space proteins in the NaCl and the guanidine extracts is shown in Fig. 2, *A* and *B*. As expected, the denaturing guanidine extracts were par-

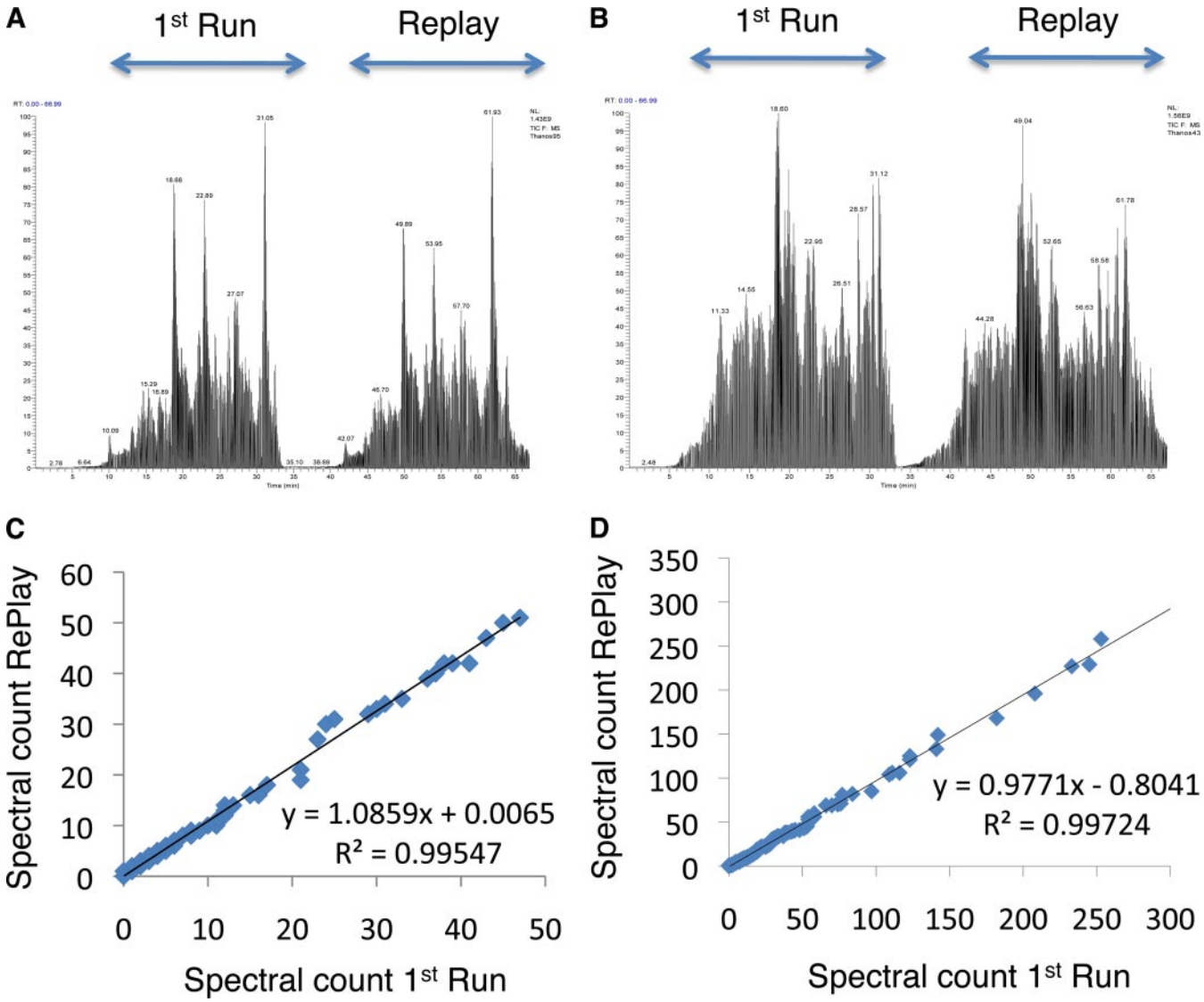

FIG. 4. **Evaluation of RePlay analysis.** Representative chromatograms for a NaCl (*A*) and a guanidine extract (*B*) using RePlay are shown. The RePlay device allows the reanalysis of the same sample during a single LC-MS/MS run. The combined correlation of the spectral counts obtained by RePlay in the three NaCl extracts (*C*) and in the three guanidine extracts (*D*) demonstrates the good correlation between the technical replicates (Correlation for each of the six extrats can be found in supplemental Fig. 3.). No RePlay analysis was performed for the SDS extracts.

ticularly enriched in ECM proteoglycans and glycoproteins (50%), whereas the mildly dissociative NaCl extracts were enriched in proteases and protease inhibitors (21%), indicating the importance of this subproteome for studying proteolytic processes in tissues.

To identify proteins of the extracellular space extracted by 0.08% SDS, we performed proteomics analysis of the SDS extracts. Because of the increased complexity of these samples, tryptic peptides were injected into a dual pressure, linear ion trap (LTQ Velos, Thermo Fisher Scientific) with faster scan speed. As expected, the majority of the identified proteins were cellular (data not shown), and only 28 extracellular space proteins were identified (Table III). The classification of the identified extracellular space proteins in the SDS extracts is shown in Fig. 2*C*. Interestingly, apart from type XIV collagen, all other extracellular space proteins have been previously identified by proteomics in the vasculature. Also, of note is the absence of proteases and protease inhibitors in these extracts either because they are obscured by abundant cellular proteins or because those that remain in the tissue following 0.5 M NaCl extraction are tightly bound to the ECM and require dissociative conditions to be extracted (*i.e.* guanidine). Peptides of extracellular space proteins identified by LC-MS/MS in the SDS extracts are shown in supplemental Table 3.

Identification of Podocan, Sclerostin, and Agrin—Among the identified proteins in the NaCl and guanidine extracts were three recently discovered glycoproteins that have never been

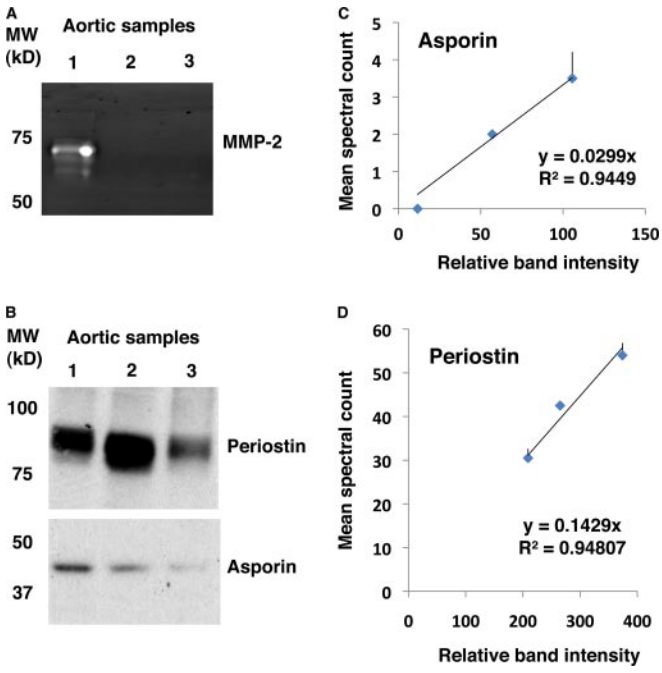

FIG. 5. **Validation of proteomics data.** Gelatin zymography confirmed the presence of MMP-2 in one of the three NaCl extracts (*A*). Periostin (*B*, *upper panel*) and asporin (*B*, *bottom panel*) were validated by immunoblotting in the guanidine extracts (on the same blotting membrane; first, asporin; and second, reprobing for periostin). The total protein loading control for the extracts can be seen in Fig. 1*C*, *bottom panel*. For periostin and asporin, the relative band intensity of the immunoblots was measured, and the values were correlated with the spectral counts of the original and the RePlay analysis ($n = 2$, mean ± S.D. *Error bars* denote standard deviation.) (*C* and *D*).

detected in the aortic ECM at the protein level. Podocan, an atypical proteoglycan, which has so far been found in the basement membrane of the glomeruli as a product of kidney podocytes (19), was detected in the NaCl extracts. Immunohistological staining confirmed the presence of podocan in the aortic intima (Fig. 3*A*; the isotype negative control is shown in Fig. 3*B*). Sclerostin, a potent bone morphogenetic protein antagonist secreted by osteoblasts and osteocytes (20), was identified in the guanidine extract and was localized in the subendothelial layer of the aortic intima (Fig. 3*C*; the isotype negative control is shown in Fig. 3*D*). The function of these glycoproteins in the vasculature is to date unknown. Finally, agrin is a large heparan sulfate proteoglycan. It has been found in the basement membrane of various tissues and is known to participate in the organization of the neuromuscular junction (21). Immunohistochemical staining confirmed the presence of agrin on the aortic endothelium (Fig. 3*E*; the isotype negative control is shown in Fig. 3*F*), which is also the site for the accumulation of other heparan sulfate proteoglycans, such as perlecan (22). It is therefore possible that agrin participates in the formation of the vascular endothelial barrier. Representative MS/MS spectra for the three glycoproteins are shown in supplemental Fig. 2.

Evaluation of RePlay—For the wider application of proteomics in clinical research, it is essential to maximize the information obtained from valuable clinical samples. Given the scarcity of human tissue available, we used the RePlay device (Advion), which allowed us to obtain a technical replicate from each clinical specimen in a single LC-MS/MS run. Representative examples of chromatograms using RePlay are shown in Fig. 4, *A* and *B*. Correlation analyses of the spectral counts in the three NaCl extracts and the three guanidine extracts are presented in Fig. 4, *C* and *D*. The mean spectral counts for the NaCl and the guanidine extracts were 32.7 ± 9.9 (median, 9.5) and 126.5 ± 41 (median, 40), respectively. The R^2 values (Pearson correlation coefficient) from all six extracts exceeded 0.94 (p values <0.001), demonstrating good reproducibility in the duplicate analyses (supplemental Fig. 3).

Because of their scarcity, MMPs are rarely detected by tissue proteomics (23). Our subfractionation, however, enabled us to obtain spectral evidence for the presence of MMP-2 in one of the NaCl extracts (aortic sample 1). Consistent with our proteomics data, gelatin zymography confirmed the presence of MMP-2 in this sample (Fig. 5*A*). A representative MS/MS spectrum for MMP-2 is shown in supplemental Fig. 4A. Importantly, the non-denaturing composition of the NaCl buffer allowed the detection of MMP-2 directly without further processing of the extracts.

In the guanidine extracts, we performed Western immunoblotting for the ECM protein periostin, which was unambiguously identified (Fig. 5*B*, *upper panel*). Periostin mRNA was recently shown to be expressed in rat carotid arteries following balloon injury (24). We also confirmed the presence of the scarce glycoprotein asporin in the vascular ECM (Fig. 5*B*, *bottom panel*). Its biological role is to date unclear, but it was recently shown to inhibit TGFβ-induced chondrogenesis in articular cartilage (25) and is a potential regulator of collagen mineralization (26). Finally, the Western blots for periostin and asporin were analyzed by densitometry, and the densitometry values were correlated with the spectral counts obtained from the RePlay analysis ($n = 2$, mean ± S.D.) (Fig. 5, *C* and *D*). Although the technical replicates obtained using the RePlay device were accurate, there is expected variability in the different clinical samples. Representative MS/MS spectra for periostin and asporin are shown in supplemental Fig. 4, B and C.

Proteolysis—Finally, we investigated whether the NaCl extract represents a subproteome enriched in degradation products. Currently, our understanding of ECM proteolysis is based on *in vitro* experiments, which do not necessarily relate to *in vivo* processes. In our methodology, the original molecular mass distribution of the identified proteins is preserved by the gel LC-MS/MS approach. Thus, our method can be important for advancing our understanding of protein degradation *in vivo*. For instance, we noted that in a fourth aortic specimen, which was classified as normal upon aortotomy, the coefficient of variation for the number of fibronectin spectra in the NaCl extract exceeded 100%, implying a significant

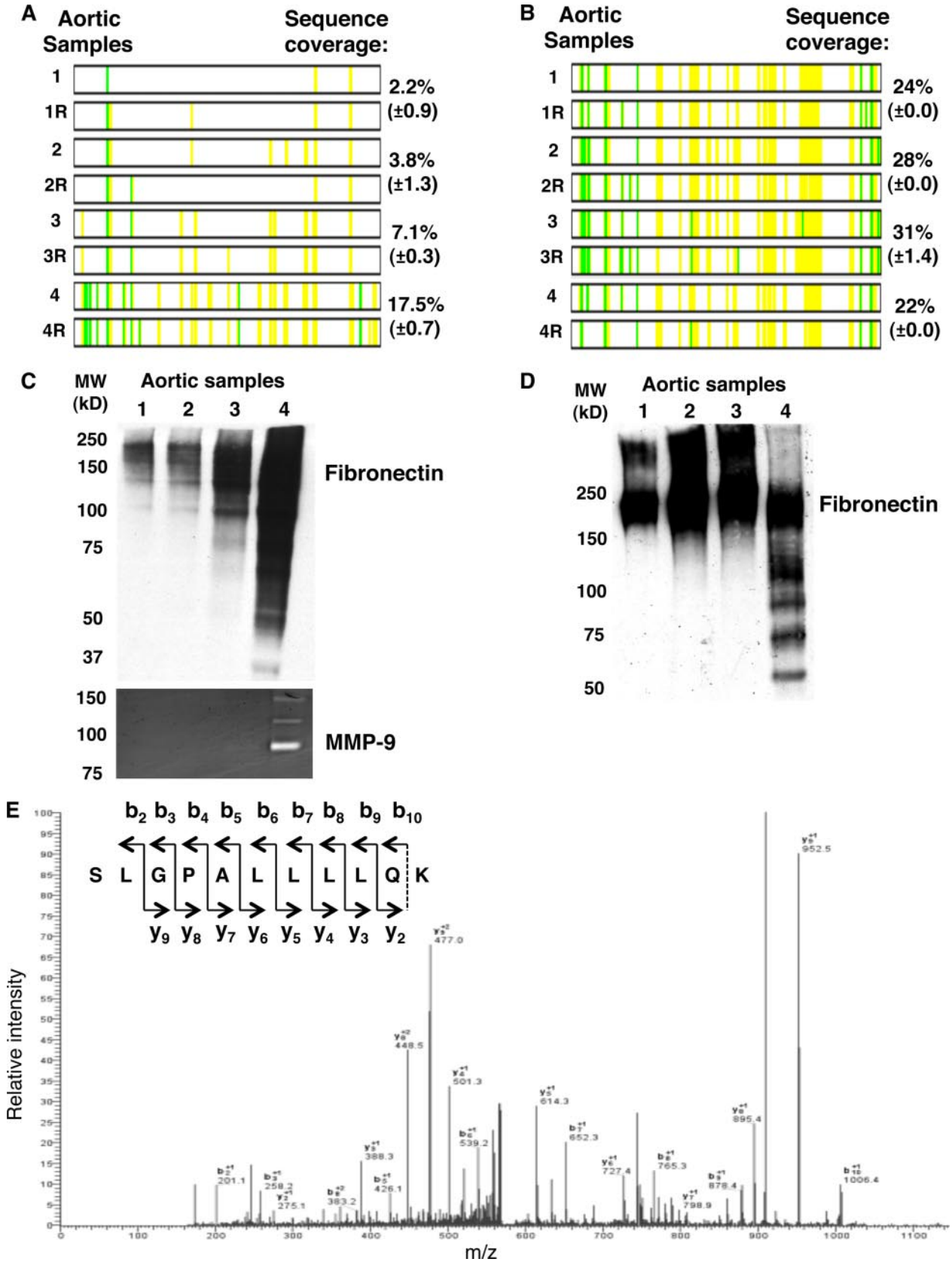
A
Aortic Samples
Sequence coverage:
1
1R
2
2R
3
3R
4
4R
2.2% (±0.9)
3.8% (±1.3)
7.1% (±0.3)
17.5% (±0.7)
B
Aortic Samples
Sequence coverage:
24% (±0.0)
28% (±0.0)
31% (±1.4)
22% (±0.0)
C
MW (kD)
Aortic samples
Fibronectin
MMP-9
D
Fibronectin
E
Relative intensity
m/z

difference in the dispersion of the data among the analyzed samples (p ANOVA <0.05). On the other hand, the coefficient of variation for samples 1–3 is not significant (58%; p ANOVA >0.05). We also noted that there was an increase in fibronectin sequence coverage (Fig. 6, *A* and *B*) and total fibronectin spectra (~4-fold) in the NaCl extract of the fourth specimen. Closer inspection of the molecular mass distribution of fibronectin spectra indicated the breakdown of fibronectin in this particular sample with more than 80% of fibronectin spectra identified in gel bands below 150 kDa. Western blotting using an antibody raised against full-length human fibronectin confirmed extensive laddering of the glycoprotein in both the NaCl and guanidine extracts (Fig. 6, *C* and *D*). Fibronectin degradation products have been implicated in the induction of proinflammatory responses in the vasculature and other tissues (1). Interestingly, mass spectrometry provided spectral evidence for MMP-9 only in this particular sample (Fig. 6*E*), and the presence of MMP-9 was confirmed by gelatin zymography (Fig. 6*C*, *lower panel*). Fibronectin is a known substrate for MMP-9 (27), but obviously, we cannot exclude that other proteinases contribute to the breakdown of fibronectin in this specimen *in vivo*. The example, however, demonstrates the potential of our methodology to analyze proteolytic activity based on the presence of proteolytic enzymes and corresponding degradation products in tissues. Importantly, this key information on protein breakdown within clinical samples that were considered normal macroscopically could be lost by using a conventional shotgun proteomics approach.

DISCUSSION

In this study, we combined biochemical fractionation with proteomics to comprehensively characterize the protein composition of the vascular extracellular environment. The main advantage of our methodology is the stepwise approach, which results in the isolation of proteins and protein degradation products loosely bound to the ECM in the NaCl fraction, the depletion of cellular proteins in the SDS fraction, and the effective solubilization of ECM proteins in the guanidine fraction.

Comprehensive Matrix Analysis—Until now, a comprehensive analysis of extracellular space components comprising the vascular proteome in humans has not been performed. Previous attempts to utilize the analytical power of proteomics to study ECM components and associated proteins have been limited by the fact that without prefractionation cellular and plasma proteins in mammalian tissues overwhelm the analytical capacities of the instruments and obscure the identification of scarce proteins in the extracellular environment. Therefore, it is not surprising that all extracellular space proteins found in the SDS extracts (except from type XIV collagen) have been reported before by proteomics studies of different vascular tissues.

On the other hand, the tissue subfractionation resulted in the identification of numerous proteins in the NaCl and guanidine extracts, which have not been investigated in the vasculature until now. The relative insolubility and the extensive post-translational modifications, especially glycosylation, render ECM proteins difficult to analyze. For example, we identified and validated the presence of three glycoproteins: podocan, originally described as a glycoprotein secreted by kidney podocytes; sclerostin, another small glycoprotein, which has recently received attention because of its ability to act as a potent negative regulator of bone morphogenetic protein signaling and bone mineralization; and agrin, a large basement membrane proteoglycan, which participates in the organization of the synapses in the neuromuscular junction. We also identified and validated the presence of the atypical proteoglycan asporin in our aortic extracts.

Moreover, the NaCl and guanidine extracts contained two ECM glycoproteins, tenascin-X and AEBP1. The first is believed to be a modulator of collagen fibrillogenesis (28). Interestingly, genetic deletion of tenascin-X in mice resulted in increased activity of MMP-2 and -9 (29). Less is known about AEBP1; the extracellular isoform was originally found to play a role in wound healing (30), and more recently, Majdalawieh *et al.* (31) showed that intracellular AEBP1 represses macrophage cholesterol efflux.

Among collagens, collagen VI appears to be very abundant in our extracts. It serves mainly as a substrate for the attachment of cells and matrix molecules and also anchors basement membranes to underlying connective tissues (32). More interesting, however, is the identification of type XIV collagen (33). Previous proteomics studies probably failed to identify this collagen because it is heavily modified by chondroitin sulfate saccharides *in vivo* (34). These modifications greatly increase its size and alter its electrophoretic properties but are removed by the deglycosylation step in our extraction methodology.

Finally, many scarce proteins, including LIM and cysteine-rich domains protein 1 (LMCD1), target of Nesh-SH3 (TARSH), and RPE-spondin (a previously hypothetical pro-

FIG. 6. **Detection of proteolysis.** Percent sequence coverage for fibronectin in the NaCl (*A*) and guanidine extracts (*B*) is shown. "*R*" denotes RePlay analysis. Note the increase of fibronectin products in the NaCl extracts of the fourth aortic specimen. Western immunoblotting of fibronectin in the NaCl (*C*) and guanidine (*D*) extracts confirmed the laddering of fibronectin. The product ion spectrum of the doubly charged tryptic peptide SLGPALLLLQK was identified as MMP-9 (*E*) (peptide probability, 95%; SEQUEST XCorr score, 2.67; SEQUEST ΔCn score, 0.40; observed m/z, 576.87; actual peptide mass, 1,151.73 Da; peptide charge, 2; delta amu, 0.0049; delta ppm, 4.3; peptide start index, 66; peptide stop index, 76). MMP-9 was only detected by LC-MS/MS in the NaCl extract of the fourth aortic specimen. Gelatin zymography confirmed higher levels of MMP-9 in this sample (*C*, *bottom panel*).

tein (35)), were all identified for the first time by proteomics in the vasculature, and representative MS/MS spectra are shown in supplemental Fig. 5. Their function in the vasculature is unknown.

The subfractionation presented here could be an important tool for studying catabolic processes in tissues. In the NaCl fraction, we found fibronectin degradation products and the presence of MMP-2 and -9 as verified by gelatinolytic zymography. Mass spectrometry also identified two mast cell proteases, namely chymase and tryptase β-1. The first was recently found to participate in the development of mouse abdominal aneurysm (36), whereas the second, an activator of MMP-3 (37), has been shown to degrade the antiatherogenic high density lipoprotein (HDL) (38). Their presence in the aortic extracts might suggest an early involvement of mast cells in aortic pathology (39).

Application to Clinical Samples—As far as vascular research is concerned, the methodical and accurate characterization of the vascular extracellular environment is essential to advance our understanding of the ECM composition in different vascular territories and their predisposition to disease processes. For instance, atherosclerosis, the major cause for morbidity and mortality in the developed world, is intimately related to dynamic changes in the ECM and its associated proteins: the retention of lipoproteins by proteoglycans leads to the development of atherosclerotic lesions, but ultimately, it is the breakdown of ECM that facilitates plaque ruptures, triggering the onset of clinical symptoms. These changes, if comprehensively characterized, could lead to new therapeutic options for cardiovascular disease. Finally, because metabolic labeling cannot be used with clinical samples, spectral counting is an alternative method to assess relative protein abundance (40), but its accuracy is poor for proteins with low spectral counts (41).

In conclusion, the proteomics method described allowed (*a*) the identification of scarce proteins present in the vascular extracellular space, (*b*) the identification of novel glycoproteins, and (*c*) the interrogation of proteolytic activity within tissues based on the identification of proteolytic enzymes and corresponding degradation products. Because ECM proteins accumulate in tissues, mRNA transcripts do not correspond to actual protein levels. In contrast, a proteomics-led approach has the potential to provide a more comprehensive analysis of the ECM composition and shed new light on pathological disease processes.

* This work was supported in part by grants from the Oak Foundation and the British Heart Foundation.

S This article contains supplemental Figs. 1–5 and Tables 1–3.

** Supported by a senior research fellowship from the British Heart Foundation. To whom correspondence should be addressed: Cardiovascular Division, King's British Heart Foundation Centre, King's College London School of Medicine, King's College London, 125 Coldharbour Lane, London SE5 9NU, UK. Tel.: 44-20-7848-5238; E-mail: manuel.mayr@kcl.ac.uk.

REFERENCES

1. Didangelos, A., Simper, D., Monaco, C., and Mayr, M. (2009) Proteomics of acute coronary syndromes. *Curr. Atheroscler. Rep.* **11,** 188–195
2. Talusan, P., Bedri, S., Yang, S., Kattapuram, T., Silva, N., Roughley, P. J., and Stone, J. R. (2005) Analysis of intimal proteoglycans in atherosclerosis-prone and atherosclerosis-resistant human arteries by mass spectrometry. *Mol. Cell. Proteomics* **4,** 1350–1357
3. Mayr, M., Chung, Y. L., Mayr, U., Yin, X., Ly, L., Troy, H., Fredericks, S., Hu, Y., Griffiths, J. R., and Xu, Q. (2005) Proteomic and metabolomic analyses of atherosclerotic vessels from apolipoprotein E-deficient mice reveal alterations in inflammation, oxidative stress, and energy metabolism. *Arterioscler. Thromb. Vasc. Biol.* **25,** 2135–2142
4. Mayr, M., Zampetaki, A., Sidibe, A., Mayr, U., Yin, X., De Souza, A. I., Chung, Y. L., Madhu, B., Quax, P. H., Hu, Y., Griffiths, J. R., and Xu, Q. (2008) Proteomic and metabolomic analysis of smooth muscle cells derived from the arterial media and adventitial progenitors of apolipoprotein E-deficient mice. *Circ. Res.* **102,** 1046–1056
5. Wu, J., Liu, W., Sousa, E., Qiu, Y., Pittman, D. D., Maganti, V., Feldman, J., Gill, D., Lu, Z., Dorner, A. J., Schaub, R., and Tan, X. Y. (2007) Proteomic identification of endothelial proteins isolated in situ from atherosclerotic aorta via systemic perfusion. *J. Proteome Res.* **6,** 4728–4736
6. Eisenstein, R., Larsson, S. E., Kuettner, K. E., Sorgente, N., and Hascal, V. C. (1975) The ground substance of the arterial wall. Part 1. Extractability of glycosaminoglycans and the isolation of a proteoglycan from bovine aorta. *Atherosclerosis* **22,** 1–17
7. Zhuang, Y., Ma, F., Li-Ling, J., Xu, X., and Li, Y. (2003) Comparative analysis of amino acid usage and protein length distribution between alternatively and non-alternatively spliced genes across six eukaryotic genomes. *Mol. Biol. Evol.* **20,** 1978–1985
8. Waanders, L. F., Almeida, R., Prosser, S., Cox, J., Eikel, D., Allen, M. H., Schultz, G. A., and Mann, M. (2008) A novel chromatographic method allows on-line reanalysis of the proteome. *Mol. Cell. Proteomics* **7,** 1452–1459
9. Keller, A., Nesvizhskii, A. I., Kolker, E., and Aebersold, R. (2002) Empirical statistical model to estimate the accuracy of peptide identifications made by MS/MS and database search. *Anal. Chem.* **74,** 5383–5392
10. Nesvizhskii, A. I., Keller, A., Kolker, E., and Aebersold, R. (2003) A statistical model for identifying proteins by tandem mass spectrometry. *Anal. Chem.* **75,** 4646–4658
11. Groves, W. E., Davis, F. C., Jr., and Sells, B. H. (1968) Spectrophotometric determination of microgram quantities of protein without nucleic acid interference. *Anal. Biochem.* **22,** 195–210
12. Mason, R. M., and Mayes, R. W. (1973) Extraction of cartilage proteinpolysaccharides with inorganic salt solutions. *Biochem. J.* **131,** 535–540
13. Dahl, S. L., Koh, J., Prabhakar, V., and Niklason, L. E. (2003) Decellularized native and engineered arterial scaffolds for transplantation. *Cell Transplant.* **12,** 659–666
14. Korossis, S. A., Wilcox, H. E., Watterson, K. G., Kearney, J. N., Ingham, E., and Fisher, J. (2005) In-vitro assessment of the functional performance of the decellularized intact porcine aortic root. *J. Heart Valve Dis.* **14,** 408–422
15. Gilbert, T. W., Sellaro, T. L., and Badylak, S. F. (2006) Decellularization of tissues and organs. *Biomaterials* **27,** 3675–3683
16. Izano, E. A., Wang, H., Ragunath, C., Ramasubbu, N., and Kaplan, J. B. (2007) Detachment and killing of Aggregatibacter actinomycetemcomitans biofilms by dispersin B and SDS. *J. Dent. Res.* **86,** 618–622
17. Tan, A., Ziegler, A., Steinbauer, B., and Seelig, J. (2002) Thermodynamics of sodium dodecyl sulfate partitioning into lipid membranes. *Biophys. J.* **83,** 1547–1556
18. Sajdera, S. W., and Hascall, V. C. (1969) Proteinpolysaccharide complex from bovine nasal cartilage. A comparison of low and high shear extraction procedures. *J. Biol. Chem.* **244,** 77–87
19. Ross, M. D., Bruggeman, L. A., Hanss, B., Sunamoto, M., Marras, D., Klotman, M. E., and Klotman, P. E. (2003) Podocan, a novel small leucine-rich repeat protein expressed in the sclerotic glomerular lesion of experimental HIV-associated nephropathy. *J. Biol. Chem.* **278,** 33248–33255
20. Sutherland, M. K., Geoghegan, J. C., Yu, C., Turcott, E., Skonier, J. E., Winkler, D. G., and Latham, J. A. (2004) Sclerostin promotes the apoptosis of human osteoblastic cells: a novel regulation of bone formation. *Bone* **35,** 828–835

21. Ngo, S. T., Noakes, P. G., and Phillips, W. D. (2007) Neural agrin: a synaptic stabiliser. *Int. J. Biochem. Cell Biol.* **39,** 863–867
22. Segev, A., Nili, N., and Strauss, B. H. (2004) The role of perlecan in arterial injury and angiogenesis. *Cardiovasc. Res.* **63,** 603–610
23. Bregant, S., Huillet, C., Devel, L., Dabert-Gay, A. S., Beau, F., Thai, R., Czarny, B., Yiotakis, A., and Dive, V. (2009) Detection of matrix metalloproteinase active forms in complex proteomes: evaluation of affinity versus photoaffinity capture. *J. Proteome Res.* **8,** 2484–2494
24. Lindner, V., Wang, Q., Conley, B. A., Friesel, R. E., and Vary, C. P. (2005) Vascular injury induces expression of periostin: implications for vascular cell differentiation and migration. *Arterioscler. Thromb. Vasc. Biol.* **25,** 77–83
25. Nakajima, M., Kizawa, H., Saitoh, M., Kou, I., Miyazono, K., and Ikegawa, S. (2007) Mechanisms for asporin function and regulation in articular cartilage. *J. Biol. Chem.* **282,** 32185–32192
26. Kalamajski, S., Aspberg, A., Lindblom, K., Heinegård, D., and Oldberg, A. (2009) Asporin competes with decorin for collagen binding, binds calcium and promotes osteoblast collagen mineralization. *Biochem. J.* **423,** 53–59
27. Ram, M., Sherer, Y., and Shoenfeld, Y. (2006) Matrix metalloproteinase-9 and autoimmune diseases. *J. Clin. Immunol.* **26,** 299–307
28. Mao, J. R., Taylor, G., Dean, W. B., Wagner, D. R., Afzal, V., Lotz, J. C., Rubin, E. M., and Bristow, J. (2002) Tenascin-X deficiency mimics Ehlers-Danlos syndrome in mice through alteration of collagen deposition. *Nat. Genet.* **30,** 421–425
29. Matsumoto, K., Takayama, N., Ohnishi, J., Ohnishi, E., Shirayoshi, Y., Nakatsuji, N., and Ariga, H. (2001) Tumour invasion and metastasis are promoted in mice deficient in tenascin-X. *Genes Cells* **6,** 1101–1111
30. Layne, M. D., Yet, S. F., Maemura, K., Hsieh, C. M., Bernfield, M., Perrella, M. A., and Lee, M. E. (2001) Impaired abdominal wall development and deficient wound healing in mice lacking aortic carboxypeptidase-like protein. *Mol. Cell. Biol.* **21,** 5256–5261
31. Majdalawieh, A., Zhang, L., Fuki, I. V., Rader, D. J., and Ro, H. S. (2006) Adipocyte enhancer-binding protein 1 is a potential novel atherogenic factor involved in macrophage cholesterol homeostasis and inflammation. *Proc. Natl. Acad. Sci. U.S.A.* **103,** 2346–2351
32. Lampe, A. K., and Bushby, K. M. (2005) Collagen VI related muscle disorders. *J. Med. Genet.* **42,** 673–685
33. Eyre, D. (2002) Collagen of articular cartilage. *Arthritis Res.* **4,** 30–35
34. Watt, S. L., Lunstrum, G. P., McDonough, A. M., Keene, D. R., Burgeson, R. E., and Morris, N. P. (1992) Characterization of collagen types XII and XIV from fetal bovine cartilage. *J. Biol. Chem.* **267,** 20093–20099
35. Schulz, H. L., Rahman, F. A., Fadl El Moula, F. M., Stojic, J., Gehrig, A., and Weber, B. H. (2004) Identifying differentially expressed genes in the mammalian retina and the retinal pigment epithelium by suppression subtractive hybridization. *Cytogenet. Genome Res.* **106,** 74–81
36. Sun, J., Zhang, J., Lindholt, J. S., Sukhova, G. K., Liu, J., He, A., Abrink, M., Pejler, G., Stevens, R. L., Thompson, R. W., Ennis, T. L., Gurish, M. F., Libby, P., and Shi, G. P. (2009) Critical role of mast cell chymase in mouse abdominal aortic aneurysm formation. *Circulation* **120,** 973–982
37. Deliargyris, E. N., Upadhya, B., Sane, D. C., Dehmer, G. J., Pye, J., Smith, S. C., Jr., Boucher, W. S., and Theoharides, T. C. (2005) Mast cell tryptase: a new biomarker in patients with stable coronary artery disease. *Atherosclerosis* **178,** 381–386
38. Lee, M., Sommerhoff, C. P., von Eckardstein, A., Zettl, F., Fritz, H., and Kovanen, P. T. (2002) Mast cell tryptase degrades HDL and blocks its function as an acceptor of cellular cholesterol. *Arterioscler. Thromb. Vasc. Biol.* **22,** 2086–2091
39. Metzler, B., and Xu, Q. (1997) The role of mast cells in atherosclerosis. *Int. Arch. Allergy Immunol.* **114,** 10–14
40. Liu, H., Sadygov, R. G., and Yates, J. R., 3rd (2004) A model for random sampling and estimation of relative protein abundance in shotgun proteomics. *Anal. Chem.* **76,** 4193–4201
41. Old, W. M., Meyer-Arendt, K., Aveline-Wolf, L., Pierce, K. G., Mendoza, A., Sevinsky, J. R., Resing, K. A., and Ahn, N. G. (2005) Comparison of label-free methods for quantifying human proteins by shotgun proteomics. *Mol. Cell. Proteomics* **4,** 1487–1502